A Cortical Activity Localization Approach for Decoding Finger Movements from Human Electrocorticogram Signal

Seyede Mahya Safavi[1], Alireza S. Behbahani[1], Ahmed M. Eltawil[1], Zoran Nenadic[2], An H. Do[2]

***Abstract*—A novel approach for decoding the finger flexion and extension from the human electrocorticogram is proposed. First, for different finger movements, we use projected MUltiple SIgnal Classification (projected MUSIC) as a source localization technique to estimate the active areas in the primary motor cortex. Next, in order to distinguish between the flexion and extension, the results of the single-trial-based source localizations are fed as the input features to a classifier for decoding. The performance of different techniques such as Support Vector Machine (SVM), Perceptron, and the k-Nearest-Neighbor (kNN) are investigated and the resulting classification accuracies are 71.59, 79.1, and 86.33 respectively.**

I. Introduction

Brain-computer interface (BCI) is a promising technique for extremity movement restoration in patients with paralysis or severe muscle disabilities. This technique extracts information originating in the human brain to recognize the intent of the user and issues appropriate commands to the external system e.g. prosthesis [1].

Recently there has been an extensive research effort devoted to the development of real-time algorithms for decoding limb movements using different modalities of the cortical signal, such as electroencephalogram (EEG), electrocoticogram (ECoG), and local field potential (LFP) [2-4]. The focus has mainly been on predicting the 3D arm movement trajectory, detecting the onset and classification of individual finger movement, and decoding the kinematics of hand and wrist movements [1], [5]. The authors in [5] use the action potentials recorded by cortex-pentetraing electrodes to show there exist groups of neurons located in specific regions of the motor cortex whose activities are highly correlated with particular hand movements. However, since the anatomical location of these task-specific neurons is fairly distributed over the primary motor cortex, some task-related areas might not be covered by commonly-sized microelectrodes. Hence, comprehensive acquisition of signals corresponding to the various hand movements using microelectrode arrays could be difficult. In addition, the cortex-penetrating nature of microelectrodes carries a number of health risks for human implantation.

ECoG signal is acquired using electrodes implanted on the surface of the brain. Therefore, a larger population of neurons can be sampled, which makes ECoG suitable for decoding the kinematics of different upper limb movements. Moreover due to its less invasive nature, ECoG electrodes are considered safer for human implantation. On the other hand, ECoG holds many advantages over non-invasive recording modalities such as EEG. These include a higher signal to noise ratio, and higher spatial and temporal resolutions. The authors in [7] have investigated the feasibility of decoding finger flexion and extension using human ECoG signals. The feasibility of predicting the direction of hand reaching movement before its onset and estimating individual finger positions in deliberately slow grasping movement using ECoG signals have been investigated in [8], [9].

It is known that the two tasks of finger flexion and extension are originating from two different groups of neurons located in slightly different areas of motor cortex[5]. Therefore, a new method for finger movement decoding is proposed where the two dimensional Cartesian coordinates of the cortical source locations are extracted using Projected MUltiple SIgnal Classification (Proj-MUSIC) technique. Next, these centers of cortical activity are used as the distinctive input features to the classifiers to distinguish the two different tasks of finger flexion and extension in the human ECoG.

The main results of this study are:

- The centers of activity for four frequency bands of Theta, Alpha, Beta, and Gamma are extracted using Proj-MUSIC for the two tasks of finger flexion and extension.
- The centers of activity for different finger angular positions during the two finger tasks are extracted.
- The source locations corresponding to different finger positions are used to classify finger movements into flexion or extension task. To this end, the following well-known classifiers have been used: perceptron, support vector machine (SVM), and k nearest neighbor (kNN).

Notation

We shall use bold capital letters for matrices and bold lower case letters for vectors. Moreover, $(.)^T$ represents matrix or vector transposition. Also $E\{.\}$ denotes the expectation operation.

II. Algorithms

A. Experiment and ECoG Signal Acquisition

This study is approved by the Institutional Review Boards of University of California, Irvine and the Rancho Los Amigos National Rehabilitation Center. The subject was a patient

[1]S. M. Safavi, A. S. Behbahani, and A. M. Eltawil are with the Department of Electrical Engineering and Computer Science, University of California, Irvine, CA 92697-2625, USA, (e-mail: {*safavis, sshahanb, aeltawil*}*@uci.edu*).

[2]Z. Nenadic and A. H. Do are with the Department of Biomedical Engineering, University of California, Irvine, CA 92697-2625, USA, (e-mail: {*znenadic, and*}*@uci.edu*).

undergoing subdural electrode implantation for the purpose of epilepsy seizure localization. An array of 8×6 electrodes was implanted on the right frontal parietal area of the cortex as depicted in Fig. 1. The experiment involved the subject's left hand four-finger flexion and extension excluding his thumb as depicted in Fig. 2, where he performed 4 sets of repetitive finger movements. Each set contained 25 alternate repetitions of fingers flexion and extension. There was an idling period of 30 seconds between consecutive sets of movements. The ECoG data was sampled at a rate of 2048 Hz. To distinguish finger flexion from extension, the finger position, θ, and velocity, $\dot{\theta}$, were recorded by a custom-made electrogoniometer [10].

B. Proj-MUSIC Source Localization

1) ***System Model****:* Assuming the cortical activity is modeled by electric dipoles with specific moments and locations, the objective of the MUSIC algorithm is to estimate the location of the active dipoles with nonzero moments [12]. In practice however, there are some unintended cortical activities in addition to the activity of interest. The presence of unintended cortical activity degrades the performance of the MUSIC algorithm. The concept of Proj-MUSIC is to suppress the effect of interfering unintended activity to improve the localization accuracy. The idea is to extract the subspace constructing the interfering signal during the *control interval* when there is no signal of interest. Next, during the *activity interval* when the signal of interest is also present, the signal is mapped to a subspace orthogonal to the interfering subspace. As a result, the interfering components are eliminated from the signal. Formulating the above concept, the data is broken into two states of control and activity as [12]

$$\begin{array}{l} \text{Control} : \mathbf{x}_C(t) = \boldsymbol{A}_I \mathbf{s}_I(t) + \mathbf{n}_C(t) \\ \text{Activity} : \mathbf{x}_A(t) = \boldsymbol{A}_S \mathbf{s}_S(t) + \boldsymbol{A}_I \mathbf{s}_I(t) + \mathbf{n}_A(t) \end{array} , \quad (1)$$

where $\mathbf{x}_C(t)$ and $\mathbf{x}_A(t)$ are $M \times 1$ vectors representing the observed signal on M different electrodes during the control and activity periods respectively. The $M \times N_I$ matrix $\boldsymbol{A}_I$ is the lead field matrix (LFM) containing N_I vectors of dimension $M \times 1$ corresponding to the response of each dipole on the M electrodes. $\boldsymbol{A}_S$ is an $M \times N_S$ LFM representing the response of N_S dipoles of interest on M electrodes. Furthermore, $\mathbf{s}_I(t)$ and $\mathbf{s}(t)$ are the $N_I \times 1$ and $N_S \times 1$ vectors of the interferer and the intended activity dipole moments. The $\mathbf{n}_C(t)$ and $\mathbf{n}_A(t)$ are the $M \times 1$ i.i.d. noise vectors. In the control state, merely unintended interfering dipoles are present, while in the activity mode, both the dipoles of intended activity and interferers are present. Each active dipole is contributing to the electric potential observed at different electrodes. The eigenvalue decomposition of the covariance matrix of the output vector, $\mathbf{x}_A(t)$, can be represented as

$$\boldsymbol{R}_A = E\{\mathbf{x}_A(t)\mathbf{x}_A^T(t)\} = \sum_{i=1}^{M} \lambda_i \mathbf{e}_i \mathbf{e}_i^T, \quad (2)$$

where $\mathbf{e}_i$s are the eigenvectors corresponding to the eigenvalues, λ_is. If the noise and the interferers are spatially and temporally stationary, one can divide these eigenvectors into signal and noise subspace eigenvectors as

$$\boldsymbol{R} = \mathbf{E}_{S,I} \Lambda_{S,I} \mathbf{E}_{S,I} + \mathbf{E}_n \Lambda_n \mathbf{E}_n, \quad (3)$$

where $\mathbf{E}_{S,I} = \{\mathbf{e}_1, ..., \mathbf{e}_{N_{S,I}}\}$ is an $M \times N_{S,I}$ matrix containing the eigenvectors corresponding to largest $N_{S,I}$ eigenvalues referred to as the signal subspace eigenvectors. The $N_{S,I} \times N_{S,I}$ diagonal matrix $\Lambda_{S,I}$ has the largest $N_{S,I}$ eigenvalues of $\boldsymbol{R}$ as its diagonal elements. $\mathbf{E}_n$ is an $M \times (M - N_{S,I})$ matrix comprised of the rest of the eigenvectors referred to as the noise subspace eigenvectors and $\Lambda_n$is an $(M - N_{S,I}) \times (M - N_{S,I})$ diagonal matrix of its corresponding eigenvalues. Note that in the activity interval, the signal subspace comprises both the interfering and signal of interest components as opposed to the control interval, where the signal subspace comprises only the interfering components.

The objective of projection is to suppress the interferers in the activity mode signal. This is fulfilled by multiplying the activity signal vector by a projecting matrix $\mathbf{P}^{\perp}$ perpendicular to the interferer subspace as

$$\mathbf{x}'_A(t) = \mathbf{P}^{\perp} \mathbf{x}_A(t) \simeq \mathbf{P}^{\perp} \boldsymbol{A}_S \mathbf{s}_S(t) + \mathbf{P}^{\perp} \mathbf{n}_A(t), \quad (4)$$

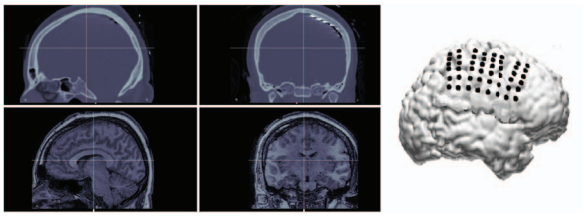

Fig. 1. The top and bottom left pictures are the post operative CT scan and the Magnetic Resonance Image (MRI) of the subject's head respectively. The left picture depicts the ECoG electrode position on the subject's right parietal frontal lobes.

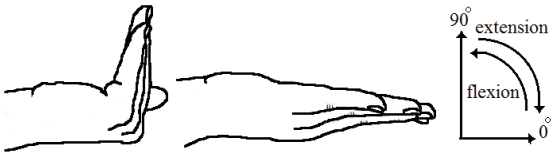

Fig. 2. The subject iteratively performed finger flexion and extension from 0 degrees, the rest position, to 90 degrees, where fingers stand perpendicular to the rest of the hand.

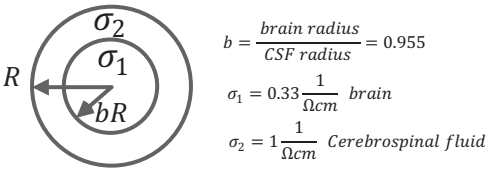

Fig. 3. The ECoG volume conduction model.

where $\mathbf{P}^{\perp} = \mathbf{I}_M - \mathbf{E}_I \mathbf{E}_I^T$ with $\mathbf{I}_M$ being an $M \times M$ identity matrix and $\mathbf{E}_I$ is an $M \times N_I$ matrix whose columns are contains the eigenvectors corresponding to largest N_I eigenvalues of control interval covariance matrix, referred to as the interfering subspace eigenvectors. The orthogonality of the projecting matrix and the interfering subspace eliminates contribution of the interferers. According to [12], the MUSIC algorithm is based on finding the locations whose lead field vectors are mostly orthogonal to the noise subspace eigenvectors $\mathbf{E}_n$ as

$$r, \boldsymbol{\varphi} = arg\ min \frac{\boldsymbol{\varphi}^T \mathbf{G}^T(r) \mathbf{E}_n \mathbf{E}_n^T \mathbf{G}(r) \boldsymbol{\varphi}}{\boldsymbol{\varphi}^T \mathbf{G}^T(r) \mathbf{G}(r) \boldsymbol{\varphi}}, \tag{5}$$

where the exhaustive search is done over all the possible dipole locations r, and dipole orientations $\boldsymbol{\varphi}$. Here, $\mathbf{G}(r)$ is the response of a dipole at location r on the M different electrodes.

Now, having $\mathbf{G}'(r) = \mathbf{P}^{\perp}\mathbf{G}(r)$, Eq. (5) can be reformulated as

$$r, \boldsymbol{\varphi} = arg\ min \frac{\boldsymbol{\varphi}^T \mathbf{G}'^T(r) \mathbf{E}'_n \mathbf{E}'^T_n \mathbf{G}'(r) \boldsymbol{\varphi}}{\boldsymbol{\varphi}^T \mathbf{G}'^T(r) \mathbf{G}'(r) \boldsymbol{\varphi}}, \tag{6}$$

where $\mathbf{E}'_n$ is obtained by eigenvalue decomposition of the covariance matrix of the new output vector $\mathbf{x}'_A(t)$.

*2) **Lead Field Matrix**:* In this paper, the brain is modeled as a sphere having two concentric shells of brain and cerebrospinal fluid (CSF) as in Fig. 3. The electric potential ν at any point $\mathbf{r}_{CSF}$ at the surface of the outer shell (i.e. CSF), can be obtained by solving the Poisson's equation as explained in [11]. The solution to the Poisson equation involves a series of weighted Legendre polynomials an associated Legendre polynomials and is formulated as an open form of

$$\nu = \frac{1}{4\pi\sigma_2 ||\boldsymbol{r}_{CSF}||^2} \sum_{n=1}^{\infty} c_n f^{n-1} \boldsymbol{m}^T \big[\boldsymbol{r}_0 P_n(cos\psi) + \boldsymbol{t}_0 \frac{P_n^1(cos\psi)}{n}\big], \tag{7}$$

where ν is the electric potential obtained at any point $\mathbf{r}_{CSF}$ on the surface of CSF due to a diploe located at $\mathbf{r}$, with respect to the center of the spheres. The 3×1 vectors $\mathbf{r}_0$ and $\mathbf{t}_0$ are vector of radial and tangential unit vectors at the point $\mathbf{r}_{CSF}$ in spherical coordinates systems. P_n and P_n^1 are Legendre and associated Legendre polynomials respectively, $\mathbf{m}$ is the dipole moment, and ψ is the angle between vectors $\mathbf{r}_{CSF}$ and $\mathbf{r}$, and $f = \frac{||\mathbf{r}||}{||\mathbf{r}_{CSF}||}$. The coefficients c_n are obtained by satisfying the boundary conditions [11].

C. Classifier

The block diagram of the proposed finger movement decoder is depicted in Fig. 4. We derive the cortical source locations corresponding to the two tasks of finger flexion and extension in a single trial based regime. Next, the Cartesian coordinates of these locations in two dimensions are given as the input features to the classifier. In this study, the performance of the SVM, the pereptron and the kNN methods were derived and compared.

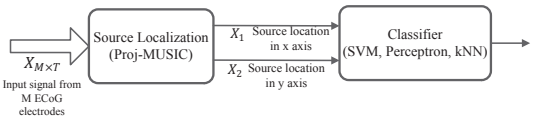

Fig. 4. Block diagram of the proposed decoder.

According to Fig. 4, the output of the source localization block is comprised of 2-dimensional Cartesian coordinates. The outputs of localization for different trials of movements is fed as the input feature to classify the type of the movement. The accuracy of classification was derived using a 100-fold cross validation. It is observed that the kNN method shows a superior performance compared to the linear classifier, where the error rate is minimum for the number of neighbors chosen to be $k = 3$.

III. Analysis

In our study, the data is investigated in two different regimes of frequency dependent and time dependent. First the ECoG data is separated based on the type of movement i.e. flexion or extension. The data in each class is further decomposed into different frequency bands using Fast Fourier Transform to trace the source locations in each of Theta (4-7 Hz), Alpha (8-12 Hz), Beta (13-30 Hz), and Gamma (ω >30 Hz) bands. Next the Proj-MUSIC is applied to the averaged data of each segment. This procedure was itetated for different trials. The centers of activity for four different frequency bands and different tasks of flexion and extension in different trials are plotted in Fig. 5. It is observed that the distinction of the source locations is more remarkable in the Gamma band which is consistent with the previous observations suggesting the Gamma band power increase during individual finger movements [6].

In the time dependent regime, we investigated the effect of finger positions on the location of sources movements. Thus, the data is first divided into different segments based on the finger angular position, where each segment belongs to a specific angular position interval of the finger. The data in each segment is further divided based on the type of movement i.e. flexion or extension. The ECoG data of a particular angular position is averaged over all trials for both tasks. Next we applied the Proj-MUSIC to the data belonging to different angular segments. The 30 seconds of idling period between consecutive sets of trials is isolated and used as the control state signal to estimate the projecting matrix $\mathbf{P}^{\perp}$. In our study, the most prominent interferer is due to the auditory activity seen in the temporal lobe. The spatial spectra of the cost function defined in Eq. 5 for thee different angular positions and different tasks of flexion and extension is plotted in Fig. 6. It is observed that the distinction of the source locations is more remarkable during the angular positions at the beginning of the tasks i.e. 6-10 degrees for the flexion and 75-80 degrees in extension.

Finally, in order to classify the acquired ECoG data, the entire data is classified into two sections. The first section belongs to the ECoG data when the subject is opening his finger.

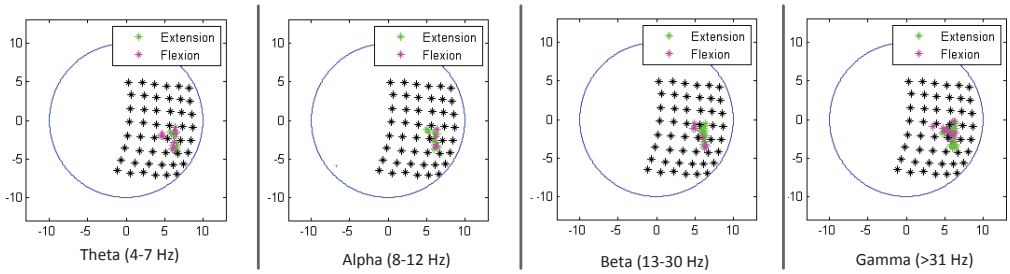

Fig. 5. The scatter plot of the estimated location of sources for flexion (purple) and extension (green) for four different frequency bands.

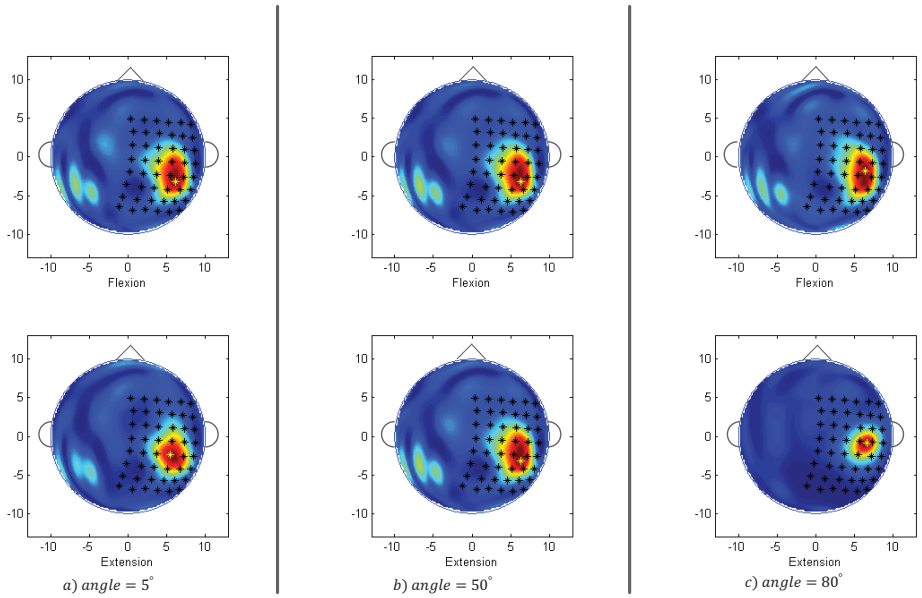

Fig. 6. Spatial spectra of the proj-MUSIC for the finger flexion (top) as well as the finger extension (bottom) for different angular positions. The average is over all trials. The black stars display the electrode positions, while the yellow stars indicate the location of the maximum cost function, which is estimated as the center of the activity.

This part of data is further split to subsections corresponding to different movement trials. The second group comprises of data during closing task and it is also divided to subsections of comprised of only a single finger flexion. Prior to application of the algorithm described earlier, the ECoG data recorded during a specific movement task interval was averaged over all samples during that particular task to create the covariance matrix of the output belonging to that movement task. The spatial spectra of the projected MUSIC as well as the position of the ECoG electrodes are depicted in Fig. 7. It is observed that the anterior central gyrus area is being more activated during the finger flexion, while the activated areas are closer to the posterior central gyrus during finger extension.

This spatial separation is the feature used in the classifier block to decode the type of movement as depicted in Fig. 8. The classification was implemented using SVM, Perceptron, and kNN methods for performance comparison. A 100-fold cross validation was done in derivation of the error rates. As Table I demonstrates the classification error rates for the three classifiers, the kNN method proves to have a better classification accuracy compared with the linear classifier. The error rate are derived with the number of neighbors being 3.

TABLE I. ERROR RATES FOR THE DIFFERENT CLASSIFICATION METHODS.

	SVM	Perceptron	kNN (k=3)
Error rates %	28.51	21.9	13.66

IV. CONCLUSION

In this study, we applied Proj-MUSIC algorithm to estimate the origin of finger flexion and extension on the surface of cortex for human ECoG signal. We investigated the effect

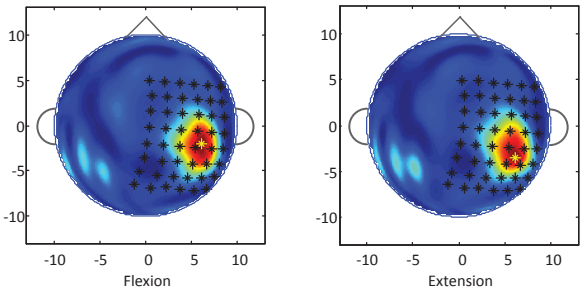

Fig. 7. Spatial spectra for the trial-based regime, where the average is over all angular positions during a single trial.

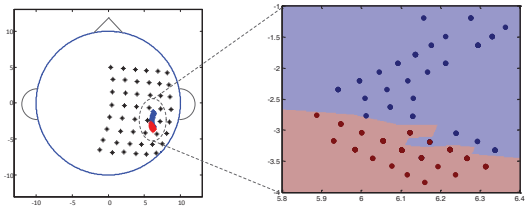

Fig. 8. The spatial separation of the source locations for two groups of tasks is used as the input feature of the classification

of finger position on the location of sources of activity as well as the location of signals containing specific frequency components. It is observed that the distinction of the two tasks of finger flexion and extension is remarkable during some specific angular positions. While the anterior central gyrus areas is more activated during the finger flexion, the posterior central gyrus region seems to be more active during finger extension. The distinction is more considerable during some of the trials. The 2-dimensional locations of the points with highest values of the cost functions were considered as the centers of the activity positions and fed as the features to the classification. The kNN neighbor classifier proves to have a 86.33 % accuracy in classifying the type of movement.

REFERENCES

[1] P. T. Wang, C. E. King, A. Schombs, J. J. Lin, M. Sazgar, F. P. K. Hsu, S. J. Shaw, D. Millett, C. Y. Liu, L. A. Chui, Z. Nenadic, and A. H. Do, Electrocorticogram encoding of upper extremity movement trajectories, in Proc 6th Int IEEE EMBS Conf Neural Eng, pp. 14291432, 2013.

[2] F. Quandta, C. Reicherta, H. Hinrichsa, H.J. Heinzea, R.T. Knightb, J.W. Riegera, Single trial discrimination of individual finger movements on one hand: A combined MEG and EEG study, Elsevier Journal on Neuroimage, Volume 59, Issue 4, 15 February 2012, Pages 33163324.

[3] W. Wang, A.D. Degenhart, J.L. Collinger, R. Vinjamuri, G.P. Sudre, P.D. Adelson, D.L. Holder, E.C. Leuthardt, D.W. Moran, M.L. Boninger, A.B. Schwartz, D.J. Crammond, E.C. Tyler-Kabara, D.J. Weber, "Human motor cortical activity recorded with Micro-ECoG electrodes, during individual finger movements," IEEE Annual International Conference of Engineering in Medicine and Biology Society, EMBC 2009, vol. 586, no. 589, pp. 3-6 Sept. 2009.

[4] V. Aggarwal, M. Mollazadeh, A.G. Davidson, M.H. Schieber, N.V. Thakor, "State-based decoding of hand and finger kinematics using neuronal ensemble and LFP activity during dexterous reach-to-grasp movements," Journal of Neurophysiology, Journal of neurophysiology 109, no. 12 (2013), pp. 3067-3081.

[5] V. Aggarwal, S. Acharya, F. Tenore, H. C. Shin, R. Etienne-Cummings, M. H. Schieber and N. V. Thakor, "Asynchronous Decoding of Dexterous Finger Movements Using M1 Neurons", IEEE Transactions on Neural Systems and Rehabilitation engineering, Vol. 16, No. 1, February 2008.

[6] M. Mollazadeh, V. Aggarwal, G. Singhal, A. Law, A. Davidson, M. Schieber, N. Thakor, "Spectral modulation of LFP activity in M1 during dexterous finger movements," IEEE 30th Annual International Conference ofIn Engineering in Medicine and Biology Society, EMBS 2008, pp. 5314-5317.

[7] M.S. Fifer, M. Mollazadeh, S. Acharya, N.V. Thakor, N.E. Crone, "Asynchronous decoding of grasp aperture from human ECoG during a reach-to-grasp task," IEEE Annual International Conference of the Engineering in Medicine and Biology Society (EMBC), pp. 4584-4587, Sept. 3 2011.

[8] Z. Wang, A. Gunduz, P. Brunner, A. L. Ritaccio, Q. Ji, G. Schalk, "Decoding onset and direction of movements using electrocorticographic (ECoG) signals in humans," Frontiers in Neuroengineering, 2012.

[9] S. Acharya, M. S. Fifer, H. L. Benz, N. E. Crone, N. V. Thakor, "Electrocorticographic amplitude predicts finger positions during slow grasping motions of the hand" Journal of neural engineering 7, vol. 4, 2010.

[10] P.T. Wang, C.E. King, A.H. Do, and Z. Nenadic, A durable, low-cost electrogoniometer for dynamic measurement of joint trajectories, Med. Eng. Phys., vol. 33(5), pp. 546-552, 2011.

[11] M. Sun, "An efficient algorithm for computing multishell spherical volume conductor models in EEG dipole source localization", IEEE Trans. Biomed. Eng., vol. 44, pp.1243 -1252 1997.

[12] Shun Chi Wu, A.L. Swindlehurst, P.T. Wang, Z. Nenadic, "Projection Versus Prewhitening for EEG Interference Suppression," IEEE Transactions on Biomedical Engineering, vol.59, no.5, pp.1329-1338, May 2012